THE JOURNAL OF PHYSICAL CHEMISTRY C

ARTICLE

pubs.acs.org/JPCC

Factors Affecting DNP NMR in Polycrystalline Diamond Samples

Leah B. Casabianca,[†] Alexander I. Shames,[‡] Alexander M. Panich,[‡] Olga Shenderova,[§] and Lucio Frydman*[,†]

[†]Department of Chemical Physics, The Weizmann Institute of Science, Rehovot 76100, Israel

[‡]Department of Physics, Ben-Gurion University, Be'er Sheva 84105, Israel

[§]International Technology Center, Raleigh, North Carolina 27617, United States

ABSTRACT: This work examines several polycrystalline diamond samples for their potential as polarizing agents for dynamic nuclear polarization (DNP) in NMR. Diamond samples of various origin and particle sizes ranging from a few nanometers to micrometers were examined by EPR, solid-state NMR and DNP techniques. A correlation was found between the size of the diamond particles and the electron spin−lattice relaxation time, the ^{13}C nuclear spin−lattice relaxation times in room temperature magic-angle-spinning experiments, and the ability of the diamond carbons to be hyperpolarized by irradiating unpaired electrons of inherent defects by microwaves at cryogenic temperatures. As the size of the diamond particles approaches that of bulk diamond, both electron and nuclear relaxation times become longer. NMR signal enhancement through DNP was found to be very efficient only for these larger size diamond samples. The reasons and implications of these results are briefly discussed, in the light of these EPR, DNP, and NMR observations.

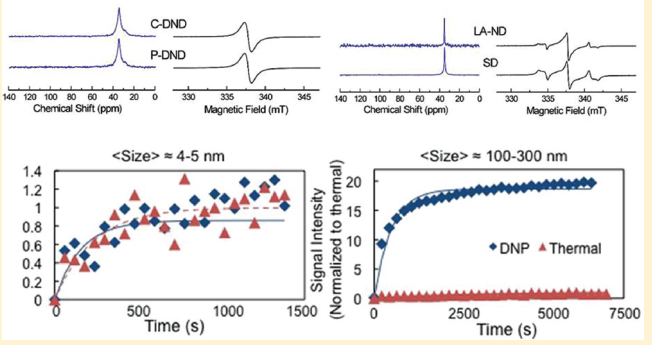

1. INTRODUCTION

Nanoscale diamonds have attracted much recent interest for their potential application[1−4] in areas ranging from quantum computing[5,6] to drug delivery[7−12] and medical imaging.[13−15] Many of these applications take advantage of the attractive NMR or EPR properties of diamonds in general, and nitrogen-vacancy (NV)-centered diamonds in particular. In general, pure diamonds have very long ^{13}C relaxation times due to the ordered carbon lattice and the low natural abundance of ^{13}C.[16,17] On the other hand, many defect sites arising either naturally or through intentional implantation of defects in diamonds supply unpaired electrons, which will shorten these nuclear relaxation times. The most common natural paramagnetic defects in diamonds include sp^3-type dangling bonds on carbons, and single nitrogen substitutions known formally as P1 (or N^0) centers. In such defects a nitrogen atom takes the place of one of the carbons in the diamond lattice and forms a long bond with one of its four carbon neighbors, containing an unpaired antibonding orbital, as well as a full bonding orbital. Another common defect involves P2 centers, consisting of a vacancy surrounded by three nitrogen substitution sites, again with an unpaired electron on a carbon adjacent to the vacancy. Also possible are N3 centers containing both nitrogen and oxygen. The nitrogen is bound to three carbons with its fourth sp^3 orbital containing a lone pair, whereas the neighboring oxygen is bound to two carbons with two lone pairs in its remaining orbitals. This results in an unpaired electron, again formally located on a carbon adjacent to the defect site. Finally, another kind of defect is the NV color center, consisting of a substitutional nitrogen adjacent to a vacancy in the carbon lattice.[18] These NV centers in particular have been the subject of much recent interest and study.[19−39] Of the six electrons in the resulting dangling bonds, two are unpaired, leading to a spin triplet. The energy levels of the NV center consist of a ^3A ground state with a splitting of ∼2.87 GHz between the $m_s = 0$ and ±1 sublevels, a ^3E excited state, and a metastable ^1A state. Electrons can be excited from the ground state to an excited state by irradiation with visible light at 532 nm. These excited electrons can relax back to the ground state either directly, or through a metastable ^1A dark state from which the electrons can only decay further into the $m_s = 0$ sublevel of the ground state. This in turn can lead to a selective population of this sublevel.[40] The ease with which these optical procedures can produce electronic hyperpolarization has opened a number of unique opportunities, particularly because this constitutes one of the few systems enabling the achievement of nearly full spin polarization at room temperature. Optical pumping of NV defect centers has permitted a number of unique optically pumped magnetic-resonance experiments, including the detection of a single electronic spin,[23−26,41−43] uses in quantum computing,[27−32,44,45] as sensitive magnetometers,[25,33−37] and for nanoscale biological imaging.[38,39]

Systems such as these ones, possessing ensembles of unpaired hyperpolarized electrons, also have potential use in the dynamic nuclear polarization (DNP) of nuclear spins. This is a technique that over the last years has gained increased popularity in the

Received: June 30, 2011
Revised: August 15, 2011
Published: September 15, 2011

Table 1. Description and ^{13}C T_1 Relaxation Times of Polycrystalline Diamond Samples

sample	description	approximate particle size	^{13}C T_1 relaxation time (s)	
			inversion recovery	saturation recovery
C-DND	as-received commercial detonation nanodiamond	4−5 nm	0.40	0.455
P-DND	purified detonation nanodiamonds, loosely aggregated powder	4−5 nm	0.80	0.377
SP-DND	superpurified and deaggregated nanodiamonds	4−5 nm	1.1	0.615
GH-DND	polycrystalline nanodiamonds prepared from a mixture of graphite and hexogen	10−30 nm	6.1	1.871
LA-ND	nanodiamond prepared by laser-ablation from carbon soot	100−300 nm	381	
SD	synthetic diamond prepared by high-pressure, high-temperature technique	microns	466	

nuclear magnetic resonance (NMR) field,[46] and which refers to the transfer of electron polarization to a bulk nuclear reservoir in order to enhance the spin polarizations, and hence the intensities, of the NMR signals. Typically, this polarization transfer takes advantage of a large electron spin polarization, achieved due to a combination of (i) the fact that separation among the electron spin energy levels is ca. 3 orders of magnitude larger than that of the nuclear energy levels and (ii) a favorable Boltzmann distribution usually achieved by low-temperature operation.[47] The ensuing transfer can be effected by irradiating the electron with microwaves in the neighborhood of their Larmor frequencies; once hyperpolarized in this manner, an enhanced nuclear NMR signal can be obtained either in the irradiated solids, or in liquids after sudden melting of the targeted sample.[48−50] Thus far a limited number of radicals have found widespread use in either kind of DNP experiments, including 1,3-bis-(diphenylene)-2-phenylallyl (BDPA), trityl derivatives, 2,2,6,6-tetramethyl-1-piperidinyloxy (TEMPO), or biradicals composed of some combination of these.[51] Also paramagnetic defects in diamond, primarily P1 and P2 centers, have been used to polarize the ^{13}C in the diamond lattice for NMR detection, at relatively low fields (0.0875, 0.35, and 1.4 T) and room temperatures.[52−55] Still, in most instances, reaching significant enhancements in nuclear polarization have demanded either low-temperature operations and/or the use of relatively high fields and thereby challenging microwave setups. It has been shown, however, that some special systems could allow one to generate high electron polarizations without having to rely on these challenging cryogenic and/or high-field setups. These include photoexcitable triplet states in organic molecular crystals,[56−62] chemically induced dynamic nuclear polarization phenomena,[63−65] and optical pumping of certain gases,[66−68] of semiconductors,[69−72] and of the above-mentioned NV-centered diamonds and nanodiamonds.[31,73] In many of these instances, reports have also been made on how the electron hyperpolarization could be transferred to nearby nuclei and exploited in hypersensitive NMR observations. Particularly attractive in this respect have been the NV-centered nanodiamond experiments reported by the Berkeley group,[20] as NV centers represent a special kind of system that could in principle be hyperpolarized at room temperature and low magnetic fields. NV centers have been optically polarized and detected using fluorescence detected magnetic resonance (FDMR) in very accessible magnetic fields, with up to 80% electron spin polarizations reported.[74] Polarization of electrons in these diamond samples has also been passed on to bulk ^{13}C by directly pumping the optical transition of the NV center; it is postulated that this polarization transfer from the unpaired electron to the bulk ^{13}C nuclei is mediated by spin diffusion effects.[20]

In this work, we examine further the prospects of relying on various inherent paramagnetic centers in diamonds to hyperpolarize nearby ^{13}C nuclei. Nanoscale or smaller diamond-like particles containing high concentrations of paramagnetic defects may be useful as polarizing agents or tracers for *in vivo* hyperpolarized NMR experiments. In this respect, it is important to understand the DNP behavior of the paramagnetic defects contained in diamonds as the nanoscale size regime is approached. To this end we have used a commercial hyperpolarizer operating at high fields and cryogenic temperatures and performed nuclear DNP by microwave irradiation at "forbidden" transition frequencies given by (electron ± nuclear) Larmor frequencies. We explored a number of different micrometer- and nanoscale diamonds, with roughly the same density of unpaired electrons. We found a size-dependence of these samples' hyperpolarizing abilities, and employed EPR and high resolution solid state ^{13}C NMR to further understand this behavior.

2. EXPERIMENTAL SECTION

Six diamond and nanodiamond samples were considered; a short description of each one is listed in Table 1. The first sample, C-DND (commercial detonation nanodiamond), is a nanodiamond powder produced at Gansu Lingyun Nano-Material Co. Ltd., Lanzhou, China, purified by oxidizing of raw detonation soot with hot nitric acid. Sample P-DND (purified detonation nanodiamond) was a loosely aggregated powder prepared by evaporating water from the colloidal solution of disintegrated purified nanodiamond of the C-DND origin, received from the NanoCarbon Research Institute, Shinshu Universtiy, Nagano, Japan. Sample SP-DND (super-purified detonation nanodiamond) was manufactured at the Ioffe Physical-Technical Institute, St. Petersburg, Russia, from an initial industrial detonation nanodiamond powder by repeatedly purifying it in boiled hydrochloric acid and then washing in boiled water as described in refs 75 and 76 for the removal of iron-containing complexes and of other para- and ferro-magnetic impurities. Sample GH-DND (graphite-hexogen detonation nanodiamond) was manufactured at the International Technology Center, Raleigh, NC, U.S.A., from a mixture of graphite and hexogen. This sample's average grain size is estimated at approximately 30 nm from SAXS measurements and at 9.6 − 13.6 nm from the XRD pattern (by the Debye−Scherrer formula). This type of nanodiamond shows larger grain sizes than those typical for DND (~4−6 nm). Sample LA-ND (laser-ablation nanodiamond) is a nanodiamond from Ray Techniques Ltd., with grain size of 100−300 nm, prepared from carbon soot by laser ablation and cleaned by flotation methods in deionized water. Sample SD (synthetic diamond) was manufactured at the Ioffe

Physical-Technical Institute, St. Petersburg, Russia, by a high pressure−high temperature (~5 GPa and 1200−1700 °C) method, using Ni−Mn and fullerenes catalysts, followed by the chemical extraction of the nanodiamonds from the obtained product and purification.

Room temperature (T = 295 K) EPR measurements were done on a Bruker EMX-220 X-band (ν = 9.4 GHz) spectrometer equipped with Agilent 53150A frequency counter. Bruker's WIN-EPR/SimFonia as well as OriginLab software were used for processing and simulation of EPR spectra. Evaluation of electron spin−lattice and spin−spin relaxation times for the paramagnetic centers found in samples under study was done using continuous microwave power saturation method. Saturation dependencies of peak-to-peak intensities were measured for the singlet 2.0028 line (all DND samples) and the central g = 2.0026 line (LA-ND and SD samples). Densities of paramagnetic centers N_s were determined by comparison with known N_s for the SP-DND sample.[76]

Dynamic nuclear polarization of the ^{13}C in diamond samples was achieved by irradiating the samples with microwaves using a 3.35 T Oxford Instruments Hypersense polarizer. For each diamond sample, between 16 and 165 mg of the solid was placed in a home-built 5-mm solids probe designed for the Hypersense. NMR experiments were done inside the 3.35 T magnet (i.e., without dissolution and transfer to a higher-field NMR magnet) using this probe, which was connected to a Varian Inova console running VNMR software. The carbon frequency at this field was 35.8813 MHz. Experiments were carried out at 1.9 K. The microwave frequency was swept from 93.975 to 94.025 GHz to find the optimum microwave frequency for each sample. Buildup of nuclear polarization under microwave irradiation was followed using small tip angle pulses (10−26°). Similar buildup curves were recorded in the absence of microwave irradiation to determine the buildup of thermal equilibrium magnetization.

Solid-state ^{13}C magic-angle-spinning (MAS) NMR spectra and relaxation times were measured at room temperature (25 C) on a Varian NMR spectrometer operating at a carbon frequency of 150.83 MHz and running VNMRJ 2.3A software. Samples were packed into 4 mm rotors and spun at 10 kHz using a Varian MAS probe, with the exception of the sample LA-ND, which was spun at 30 kHz using a 1.6 mm Varian MAS probe, and sample GH-DND, which was spun at 10 kHz using a 3.2 mm Varian MAS probe. Simple single-pulse experiments were recorded, as no difference was noted from the use of heteronuclear decoupling. To ensure a better coil filling factor, Teflon spacers were utilized in these ^{13}C MAS NMR measurements; due to the Teflon caps, spectra were corrected by subtracting from them the spectra of an empty rotor collected under the same experimental conditions. For the T_1 measurements, the inversion−recovery pulse sequence (180−τ−90−acquire) was used, and the resulting signal intensities were fitted to stretched exponentials.[77] ^{13}C T_1 measurements were also made using saturation-recovery experiments.

3. RESULTS

The room temperature solid-state ^{13}C NMR spectra of the six samples examined in this study are presented in Figure 1(a). All of the samples show a peak around 35 ppm attributed to carbons in a regular diamond lattice, for some samples a shoulder on the high field side of this sharp peak. A similar shoulder on the high field side of the sp^3 carbon peak in purified nanodiamonds was

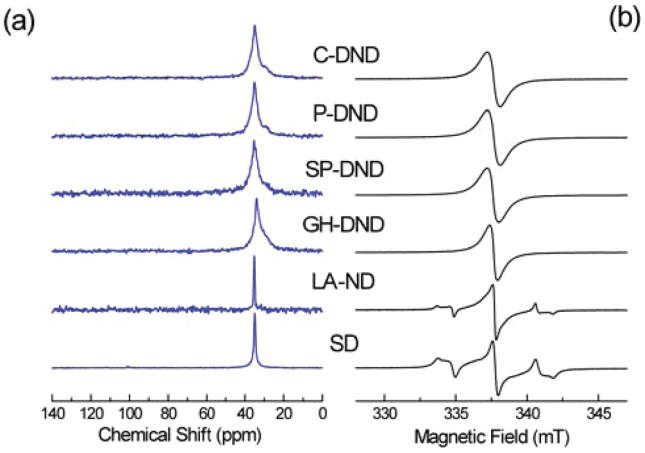

Figure 1. Room temperature solid-state ^{13}C NMR (a) and polycrystalline X-band (ν = 9.466 GHz) EPR (b) spectra of the nano- and micrometer-sized diamond samples. The NMR spectra were obtained using a one-pulse sequence with no ^{1}H- decoupling. C-DND: 15.3 mg sample, 10 kHz MAS, 2 s recycle delay, 2048 scans; P-DND: 51.5 mg sample, 10 kHz MAS, 10 s recycle delay, 256 scans; SP-DND: 27.6 mg sample, 10 kHz MAS, 10 s recycle delay, 256 scans, GH-DND: 24.0 mg sample, 10 kHz MAS, 30 s recycle delay, 256 scans; LA-DND: 10.6 mg sample, 30 kHz MAS, 1800 s recycle delay, 16 scans; SD: 126.0 mg sample, 10 kHz MAS, 1800 s recycle delay, 20 scans. In the NMR spectra for C-, S-, and SP-DND, the spectrum of an empty rotor taken under the same experimental conditions has been subtracted from the experimental spectrum of the sample. The peak near 100 ppm in the SD NMR spectrum is a spinning sideband. For better presentation intensities of all NMR and EPR spectra were normalized to their peak values.

observed by Dubois et al[78] and Belobrov et al.[79] We do not, however, observe the low-field tail observed by Fang et al[80] and attributed to disordered carbon atoms on the nanodiamond surface. Samples C-DND, P-DND, and SP-DND also show an artificial peak at 110 ppm, arising due to Teflon contributions from the sample caps. This signal is usually not seen in cross-polarization MAS NMR experiments, but it can be seen in the ^{13}C one-pulse experiments shown here. To correct for this artificial peak, spectra were taken of an empty rotor with Teflon sample caps, under the same experimental conditions. The spectra of the empty rotor have been subtracted from the spectra shown in Figure 1a for samples C-DND, P-DND, and SP-DND. The absence of this signal in the SD sample is probably due to the larger sample amounts, and hence higher sensitivities, associated to these measurements; for samples LA-ND and GH-DND, different rotors were used. Room-temperature ^{13}C T_1 measurements were made using an inversion−recovery pulse sequence and fitted to stretched exponentials. The ^{13}C T_1 values are listed in Table 1 and increase with increasing particle size. Levin et al[81] also report that the ^{13}C T_1 values in nanodiamonds are more than 3 orders of magnitude shorter than the T_1's of microdiamonds.

Representative room temperature EPR spectra for the samples under study are shown in Figure 1b. Samples C-, P-, SP-, and GH-DND show the Lorentzian-like singlet EPR signals. It was recently found[76] that the singlet Lorentzian-like signal observed in bulk DND samples at room temperature may be decomposed into two Lorentzian signals having similar g-factor values and different line widths. Examples of such decomposition are presented in Figure 2a,b. The EPR parameters of such overlapping Lorentzian signals, the ratios between the integrated intensity of the narrow line and the broad one (S_1/S_2), and the

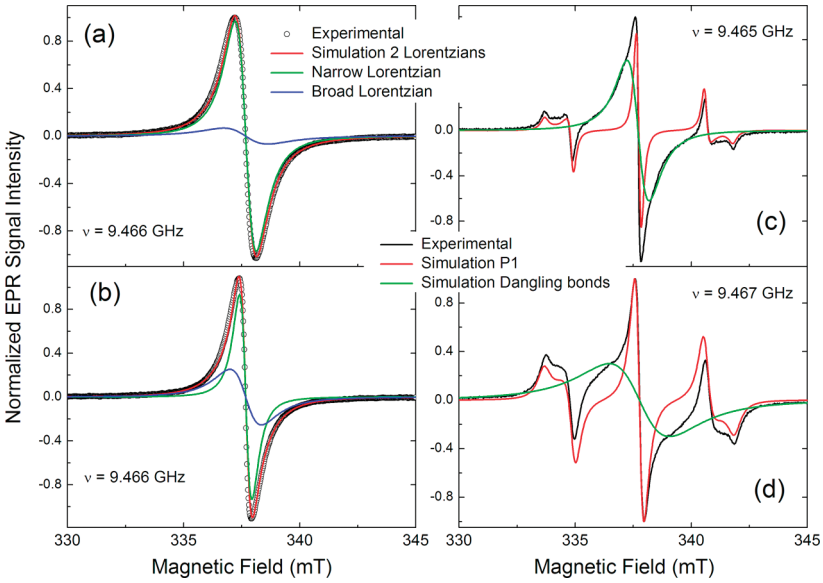

Figure 2. Room temperature X-band EPR spectra of polycrystalline diamond samples, recorded at 200 μW: well purified 4−6 nm grain size SP-DND (a) and 10−30 nm grain size GH-DND (b) samples; open circles, experimental spectrum; red line, best fit by two Lorentzian lines; green line, narrow Lorentzian line; blue line, broad Lorentzian line; 100−300 nm grain size LA-ND sample (c) and micrometer-sized SD sample HPHT (d); black line, experimental spectrum; red line, simulated spectrum of nitrogen related P1 centers; green line, simulated spectrum of carbon inherited centers.

Table 2. Room Temperature EPR and Electron Relaxation Parameters for Polycrystalline Diamond Samples

sample	g_{iso}	ΔH_{pp1} (mT)	ΔH_{pp2} (mT)	S_1/S_2	N_s (10^{19} spin/g)	A_{xx2}, A_{yy2} (mT)	A_{zz2} (mT)	$^*T_{SL1}$ (10^{-8} s)	T_{SL2} (10^{-6} s)	$^*T_{SS1}$ (10^{-9} s)	T_{SS2} (10^{-8} s)
C-DND	2.0028 ± 0.0001	0.91 ± 0.01	2.00 ± 0.08	~4	8.5 ± 0.9			5.2		7.2	
P-DND	2.0028 ± 0.0001	0.91 ± 0.01	1.99 ± 0.08	~3	6.7 ± 0.7			4.9		7.2	
SP-DND	2.0028 ± 0.0001	0.77 ± 0.01	1.64 ± 0.05	~1.2	6.3 ± 0.2			5.4		8.5	
GH-DND	2.0028 ± 0.0001	0.53 ± 0.01	1.35 ± 0.05	~0.6	4.2 ± 0.4			9.5 ± 0.5		12.4 ± 0.5	
LA-ND	2.0026 ± 0.0002	0.95 ± 0.05		~1	2.4 ± 0.3	2.86 ± 0.02	4.05 ± 0.05	4.8 ± 0.3	19 ± 2	6.9	3.2 ± 0.2
SD	2.0026 ± 0.0002	2.6 ± 0.1		~1	5.1 ± 0.5	2.86 ± 0.02	4.05 ± 0.05	72 ± 2	12 ± 1	2.5	1.7 ± 0.2

* Due to the estimation method in use (continuous saturation and fitting by eq 1) the error bars for the short relaxation times listed above may reach 30% of the values presented.

total spin densities are listed in Table 2. It is worth mentioning that the $S_1/S_2 \approx 0.6$ value for the GH-DND sample is significantly different from the corresponding values found for conventional DND (C-, P-, and SP-DND) samples, which range from 1.2 to 4. It means that, unlike conventional DND samples, in the GH-DND sample, paramagnetic centers responsible for the broad signal (shallow ones, following refs 76 and 82) prevail over centers giving the narrow line (deep ones). We ascribe this feature to the higher concentration of dangling bonds, arising in this case from the nanodiamond edges.[83]

In contrast to the aforementioned detonation-obtained ND samples, the LA-ND and SD samples demonstrate complicated EPR signals consisting of two unlike independent components which saturate at different microwave power levels. At low microwave powers, when neither component is saturated, each experimental spectrum is a superposition of a well resolved polycrystalline hyperfine pattern and a singlet Lorentzian line - red and green lines in Figure 2c,d. The polycrystalline hyperfine pattern originates from paramagnetic centers arising from a single unpaired electron anisotropically interacting with the ^{14}N nucleus (an $I = 1$) in diamond's so-called P1 or N^0 centers. The Lorentzian line originates from carbon inherited paramagnetic defects (dangling bonds). Relative intensities of signals belonging to these two types of paramagnetic centers are about the same. EPR parameters of these components are listed in Table 2.

Experimentally obtained saturation dependencies for the electron spins at room temperature are shown in Figure 3. It is clear that samples GH-DND, LA-ND, and SD show deviations from the nonsaturated linear behavior (red dotted line), at lower values of incident microwave power than conventional DND samples C-DND, P-DND, and SP-DND. Following ref 84, the saturation behavior of these peak-to-peak signal intensities Y_{pp} may be described by the relationship

$$Y_{pp} = \sum_i \frac{C_i G \sqrt{P} {T_{SSi}}^2}{(1 + G^2 P T_{SLi} T_{SSi})^{3/2}} \quad (1)$$

where i is number of overlapping components, P is the microwave power, $G = g\gamma$ (the g-factor and γ gyromagnetic ratio, respectively), and C_i, T_{SLi}, and T_{SSi} are weighting coefficients describing the electron spin−lattice and spin−spin relaxation

dx.doi.org/10.1021/jp206167j |J. Phys. Chem. C 2011, 115, 19041–19048

times for each component, respectively. Equation 1 allows an approximate quantification of differences in the electronic relaxation parameters of samples under interest. It was found that experimental data for all DND samples may be successfully simulated using a single component, $i = 1$ in eq 1, and for samples LA-ND and SD, two components, $i = 2$. The former indicates that both broad and narrow components of the singlet Lorentzian-like EPR signal have the indistinguishable electron relaxation parameters, whereas the latter correlates well with the other two types of EPR signals observed. Solid lines in Figure 3 represent best fits of saturation data for all samples. The electron spin−lattice (T_{SLi}) and spin−spin (T_{SSi}) relaxation times found by simulations are listed in Table 2.

Dynamic nuclear polarization of the diamond ^{13}C's was attempted by cooling each neat powder to cryogenic temperatures and irradiating the samples with microwaves at a frequency near the expected transition of the unpaired electron. NMR signals could be observed from these low temperature samples even in the absence of microwave irradiation. The intensity of the observed ^{13}C signal as a function of microwave frequency is shown for each sample in Figure 4. At each frequency, after saturating the magnetization using a series of 90° pulses, microwaves were turned on for 1−10 min before observing carbon magnetization. The signal intensities in Figure 4 are normalized to the signal intensity resulting from the same experiment but with microwaves off. For samples C-DND and P-DND, no significant change in signal intensity was observed over the microwave frequency range accessible to us, indicating that polarization of the unpaired electron was not successfully transferred to the diamond carbons through the solid or cross effect DNP. Only for samples LA-ND and SD was a significant positive and negative signal enhancement seen. These correspond to positive and negative spin alignments of the bulk ^{13}C of the diamond sample, as expected from a hyperpolarization mediated by DNP. As can be seen in the expanded plot in Figure 4b, samples SP-DND and GH-DND exhibited intermediate polarization transfer, resulting in enhancements of order of magnitude 10-fold or less.

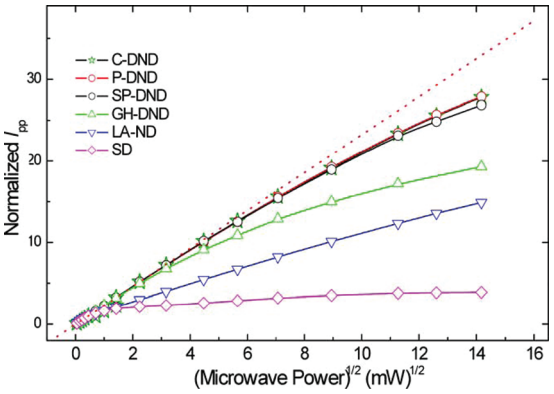

Figure 3. Saturation curves for polycrystalline diamond samples, obtained at room temperature. Symbols represent experimental data: C-DND (olive stars), P-DND (red circles), SP-DND (black circles), GH-DND (green triangles), LA-ND (blue triangles), and SD (magenta diamonds). Corresponding solid lines represent best least-squares fits by eq 1 with $i = 1$ for samples C-, P-, SP-, and GH-DND and $i = 2$ for samples LA-ND and SD. Red dotted line shows linear nonsaturating behavior.

Figure 5 shows the buildup of nuclear polarization as a function of time. The blue diamonds depict the polarization buildups under the effects of DNP, and the red triangles are the buildup of thermal equilibrium polarization at 1.9 K. Solid and dashed lines are exponential fits to these experimental points for the DNP and thermal equilibrium polarization, respectively. For the DNP, the microwave frequency and power were set at optimized levels determined for each sample. In each case, the signal intensities are normalized to the maximum intensity for thermal polarization, found from the exponential fit. Notice that only the samples LA-ND and SD have a significant gain in signal intensity under DNP. The extent of hyperpolarization that is able to be achieved is shown in the inset of Figure 5e. This figure shows ^{13}C NMR spectra of sample LA-ND at 3.35 T with and without microwave irradiation, exemplifying the signal enhancement that is seen in the solid state.

4. DISCUSSION

As can be seen from the nuclear spin−lattice relaxation data in Table 1 and the electron relaxation data in Table 2, as the characteristic length scale of the particles in each diamond sample increases, so do both the electron and nuclear spin−lattice relaxation times measured at room temperature. Here it is worth mentioning that due to the estimation method in use (continuous saturation and fitting by eq 1), the error bars for the short electron relaxation times in Table 2 may reach 30% of the

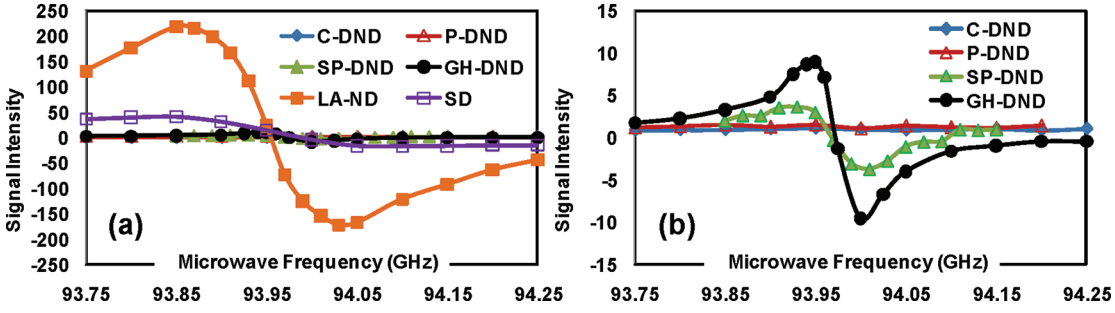

Figure 4. (a) Dependence of ^{13}C NMR signal enhancement on microwave frequency for the six samples studied. Blue diamonds: sample C-DND, 10 min polarization, 25 mW microwave power, 90° pulse; red open triangles: sample P-DND, 5 min polarization, 50 mW, 90° pulse; green triangles: sample SP-DND, 3 min polarization, 100 mW, 90° pulse; black circles: sample GH-DND, 5 min polarization, 100 mW, 90° pulse; orange squares: sample LA-ND, 2 min polarization, 40 mW, 90° pulse; purple open squares: sample SD, 1 min polarization, 60 mW, 13° pulse. Each sample was irradiated by microwaves at each frequency for the indicated time and the resulting signal intensity was normalized to the intensity of signal from the same experiment, but with microwaves off. (b) Expanded version of the same plot as in (a).

dx.doi.org/10.1021/jp206167j |J. Phys. Chem. C 2011, 115, 19041–19048

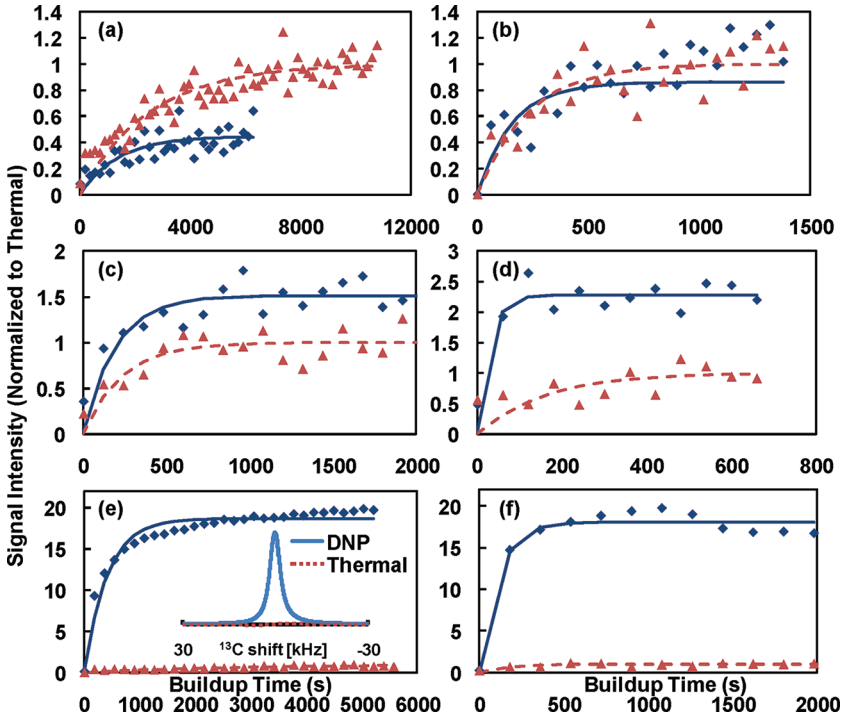

Figure 5. DNP-driven buildup of nuclear polarization. The signal intensity was measured as a function of time using small tip-angle pulses. For each plot, blue diamonds represent the signal intensity with microwaves on and red triangles represent the signal intensity with microwaves off. Solid blue and dashed red lines are exponential fits for the DNP and thermal equilibrium buildup, respectively. (a) Sample C-DND: 93.950 GHz, 75 mW microwave power, 10° pulse. (b) Sample P-DND: 93.850 GHz, 50 mW, 26° pulse; (c) Sample SP-DND: 93.930 GHz, 40 mW, 10° pulse. (d) Sample GH-DND: 93.950 GHz, 100 mW, 13° pulse. (e) Sample LA-ND: 93.850 GHz, 40 mW, 13° pulse. (f) Sample SD: 93.850 GHz, 25 mW, 13° pulse. Only the SD (f) and LA-ND (e) have a significant DNP effect, while samples SP-DND and GH-DND have intermediate DNP enhancements. The inset in (e) is the spectrum of sample LA-ND obtained following a 90°-pulse after 100 min of microwave irradiation at 93.850 GHz and 40 mW power (blue solid line) and after 100 min of thermal equilibration (red dashed line).

values found. However, even accepting such a strong uncertainty, one can clearly see that the short electron relaxation times in small DNDs (samples C-, P-, and SP-DND) lengthen upon increasing the particle size (sample GH-DND). Electron relaxation in both larger samples shows that nitrogen-related centers are characterized by significantly longer electron relaxation times (two orders for the spin−lattice relaxation time) than the carbon-related paramagnetic centers. This characteristic length scale effect may be attributed to differences in the local density of unpaired electrons and to different interactions between these paramagnetic centers in samples of various sizes and origin. This correlation between diamond particle size and electron spin−lattice relaxation (particularly of the nitrogen-based sites) may also explain our inability to observe nitrogen-related defects in the 4−6 nm sized DND by CW EPR. These samples carry a large number of unpaired spins (up to 15 per particle[76]) that are delocalized over the nano-object and coupled by strong exchange interaction. One can suppose that, on increasing the particle size, this exchange weakens (at least for some types of paramagnetic centers), leading to an increase of relaxation time in the 10−30 nm sized GH-DND samples. Further increase of nanodiamond particle size leads to additional relaxation time prolongation, revealing clear nitrogen-related signals in the CW EPR spectra of the LA-ND and SD samples.

Significant DNP enhancements of the ^{13}C NMR signal was possible only for the two samples of larger particle sizes, LA-ND and SD. Although samples C-, P-, SP-, and GH-ND exhibited a strong EPR singlet within the irradiation region of our microwave source, and although they contain unpaired electrons in high densities $\geq 10^{19}$ spins/g, microwave irradiation of this EPR line did not result in a significant polarization transfer to the bulk ^{13}C nuclei. Samples SP-DND and GH-DND have only small DNP enhancements. We ascribe this to the relaxation time characteristics of both nuclear and electron spins. Indeed, two conditions are usually needed for hyperpolarizing ^{13}C nuclei through DNP. One concerns the ability of the electron spin populations to be equalized by microwave radiation. As can be seen in Figure 3, as the sample size increases, the electron spins become more amenable to saturation, whereas the shorter electron T_1 of the smaller-size nanodiamonds drives the populations back to their Boltzmann equilibrium values. This saturation behavior also correlates with DNP efficiency: as the electron relaxation time increases, so does the DNP enhancement. A second factor compromising DNP in the smaller nanodiamond samples is related to nuclear relaxation times. DNP in bulk can be envisioned as consisting of a two-step process: the first is polarization of the "core" nuclei near the electron, while a second step is polarization of the bulk nuclei due to spin diffusion. Because the observed signal is composed primarily of the bulk nuclei, the nuclear signal enhancement depends on long nuclear T_1s enabling this spin diffusion process to build up its effects over relatively long periods. The long nuclear relaxation times that Table 1 reveals for the larger-sized diamond particles, are therefore aiding the electron polarization to be transferred to the bulk nuclei during the DNP.

5. CONCLUSION

This work examined the magnetic resonance properties of a series of nano- and micrometer-sized diamond samples containing naturally occurring nitrogen-containing defects. Correlations among the electron relaxation times, nuclear relaxation times, and hyperpolarizing efficiencies were observed, and these could be associated with the behavior observed for the diamond particle size. As the characteristic length of the diamond particles approaches that of bulk diamond, both electron and nuclear spin−lattice relaxation times increase. Dynamic nuclear polarization was only successful for these two diamond samples of largest particle sizes. The two samples of largest particle sizes also reveal a slowly relaxing EPR component with a well-defined hyperfine coupling characteristic of a single unpaired electron interacting with ^{14}N in a P1 defect center. For the smaller samples, the fast electron spin−lattice relaxation time of the EPR singlet prevents the electron spins from being saturated, and the fast nuclear spin−lattice relaxation time prevents the buildup of nuclear polarization through spin diffusion.

This work confirms that nanodiamonds may have potential as polarizing agents for DNP: at least when using a "brute force" method of irradiating unpaired electrons of naturally occurring defect sites with microwaves at cryogenic temperatures, we were able to polarize bulk ^{13}C nuclei of diamonds. The measurements also reveal that there is a correlation between the size dependence of these particles and the efficiency of the DNP effect observed as well. While smaller nanosized diamonds are attractive from the point of being useful as tracers, the good DNP properties of bulk diamond may not always be retained in these small size regimes.

AUTHOR INFORMATION

Corresponding Author

*Tel: +972-8-9344903. Fax:+972-8-9344123. E-mail: lucio.frydman@weizmann.ac.il.

ACKNOWLEDGMENT

This research was supported by the Israel Science Foundation (ISF 447/09), ERC Advanced Grant No. 246754, a Helen and Kimmel Award for Innovative Investigation, and the generosity of the Perlman Family Foundation. We thank B. Zousman (Ray Techniques Ltd., Jerusalem, Israel), E. Osawa (NanoCarbon Research Institute, Shinshu Universtiy, Nagano, Japan), and A. Ya. Vul' and V. Yu. Osipov (Ioffe Physical-Technical Institute, St. Petersburg, Russia) for providing various diamond samples. L.B.C. acknowledges postdoc fellowships from the U.S. National Science Foundation (Grant No. OISE-0965137) and the United States-Israel Educational Foundation/Fulbright commission in Israel.

REFERENCES

(1) Schrand, A. M.; Ciftan Hens, S. A.; Shenderova, O. A. *CRC Crit. Rev. Solid State Sci.* **2009**, *34*, 18–74.
(2) Krueger, A. *Chem.—Eur. J.* **2008**, *14*, 1382–1390.
(3) Baidakova, M.; Vul', A. *J. Phys. D: Appl. Phys.* **2007**, *40*, 6300–6311.
(4) Xing, Y.; Dai, L. M. *Nanomedicine* **2009**, *4*, 207–218.
(5) Barnard, A. S.; Sternberg, M. *Nanotechnology* **2007**, *18*, 025702.
(6) Holt, K. B. *Philos. Trans. R. Soc. A* **2007**, *365*, 2845–2861.
(7) Liu, K.-K.; Zheng, W.-W.; Wang, C.-C.; Chiu, Y.-C.; Cheng, C.-L.; Lo, Y.-S.; Chen, C.; Chao, J.-I. *Nanotechnology* **2010**, *21*, 315106.
(8) Li, X. X.; Shao, J. Q.; Qin, Y.; Shao, C.; Zheng, T. T.; Ye, L. *J. Mater. Chem.* **2011**, *21*, 7966–7973.
(9) Guan, B.; Zou, F.; Zhi, J. *Small* **2010**, *6*, 1514–1519.
(10) Chen, M.; Pierstorff, E. D.; Lam, R.; Li, S.-Y.; Huang, H.; Osawa, E.; Ho, D. *ACS Nano* **2009**, *3*, 2016–2022.
(11) Lam, R.; Ho, D. *Expert Opin. Drug Delivery* **2009**, *6*, 883–895.
(12) Huang, H.; Pierstorff, E.; Osawa, E.; Ho, D. *Nano Lett.* **2007**, *7*, 3305–3314.
(13) Barnard, A. S. *Analyst* **2009**, *134*, 1751–1764.
(14) Fu, C.-C.; Lee, H.-Y.; Chen, K.; Lim, T.-S.; Wu, H.-Y.; Lin, P.-K.; Wei, P.-K.; Tsao, P.-H.; Chang, H.-C.; Fann, W. S. *Proc. Natl. Acad. Sci. U.S.A.* **2007**, *104*, 727–732.
(15) Chang, Y.-R.; Lee, H.-Y.; Chen, K.; Chang, C.-C.; Tsai, D.-S.; Fu, C.-C.; Lim, T.-S.; Tzeng, Y.-K.; Fang, C.-Y.; Han, C.-C.; Chang, H.-C.; Fann, W. S. *Nat. Nanotechnol.* **2008**, *3*, 284–288.
(16) Hoch, M. J. R.; Reynhardt, E. C. *Phys. Rev. B* **1988**, *37*, 9222–9226.
(17) Reynhardt, E. C.; Terblanche, C. J. *Chem. Phys. Lett.* **1997**, *269*, 464–468.
(18) Reynhardt, E. C.; High, G. L. *Prog. Nucl. Magn. Reson. Spectrosc.* **2001**, *38*, 37–81.
(19) Wrachtrup, J.; Jelezko, F. *J. Phys.-Condens. Matter* **2006**, *18*, S807–S824.
(20) King, J. P.; Coles, P. J.; Reimer, J. A. *Phys. Rev. B* **2010**, *81*, 073201.
(21) Stanwix, P. L.; Pham, L. M.; Maze, J. R.; Le Sage, D.; Yeung, T. K.; Cappellaro, P.; Hemmer, P. R.; Yacoby, A.; Lukin, M. D.; Walsworth, R. L. *Phys. Rev. B* **2010**, *82*, 201201.
(22) Acosta, V. M.; Jarmola, A.; Bauch, E.; Budker, D. *Phys. Rev. B* **2010**, *82*, 201202.
(23) Neumann, P.; Beck, J.; Steiner, M.; Rempp, F.; Fedder, H.; Hemmer, P. R.; Wrachtrup, J.; Jelezko, F. *Science* **2010**, *329*, 542–544.
(24) Maurer, P. C.; Maze, J. R.; Stanwix, P. L.; Jiang, L.; Gorshkov, A. V.; Zibrov, A. A.; Harke, B.; Hodges, J. S.; Zibrov, A. S.; Yacoby, A.; Twitchen, D.; Hell, S. W.; Walsworth, R. L.; Lukin, M. D. *Nat. Phys.* **2010**, *6*, 912–918.
(25) Maze, J. R.; Stanwix, P. L.; Hodges, J. S.; Hong, S.; Taylor, J. M.; Cappellaro, P.; Jiang, L.; Gurudev Dutt, M. V.; Togan, E.; Zibrov, A. S.; Yocoby, A.; Walsworth, R. L.; Lukin, M. D. *Nature* **2008**, *455*, 644–648.
(26) Buckley, B. B.; Fuchs, G. D.; Bassett, L. C.; Awschalom, D. D. *Science* **2010**, *330*, 1212–1215.
(27) Neumann, P.; Kolesov, R.; Naydenov, B.; Beck, J.; Rempp, F.; Steiner, M.; Jacques, V.; Balasubramanian, G.; Markham, M. L.; Twitchen, D. J.; Pezzagna, S.; Meijer, J.; Twamley, J.; Jelezko, F.; Wrachtrup, J. *Nat. Phys.* **2010**, *6*, 249–253.
(28) Gaebel, T.; Domhan, M.; Popa, I.; Wittmann, C.; Neumann, P.; Jelezko, F.; Rabeau, J. R.; Stavrias, N.; Greentree, A. D.; Prawer, S.; Meijer, J.; Twamley, J.; Hemmer, P. R.; Wachtrup, J. *Nat. Phys.* **2006**, *2*, 408–413.
(29) Hanson, R.; Mendoza, F.; Epstein, R. J.; Awschalom, D. D. *Phys. Rev. Lett.* **2006**, *97*, 087601.
(30) Howard, M.; Twamley, J.; Wittmann, C.; Gaebel, T.; Jelezko, F.; Wrachtrup, J. *New J. Phys.* **2006**, *8*, 33.
(31) Jacques, V.; Neumann, P.; Beck, J.; Markham, M.; Twitchen, D.; Meijer, J.; Kaiser, F.; Balasubramanian, G.; Jelezko, F.; Wrachtrup, J. *Phys. Rev. Lett.* **2009**, *102*, 057403.
(32) Nizovtsev, A. P.; Kilin, S. Ya.; Jelezko, F.; Gaebal, T.; Popa, I.; Gruber, A.; Wrachtrup, J. *Opt. Spectrosc.* **2005**, *99*, 233–244.
(33) Acosta, V. M.; Bauch, E.; Jarmola, A.; Zipp, L. J.; Ledbetter, M. P.; Budker, D. *Appl. Phys. Lett.* **2010**, *97*, 174104.
(34) Bouchard, L. S.; Acosta, V. M.; Bauch, E.; Budker, D. *New J. Phys.* **2011**, *13*, 025017.
(35) Said, R. S.; Berry, D. W.; Twamley, J. *Phys. Rev. B* **2011**, *83*, 125410.
(36) Schoenfeld, R. S.; Harneit, W. *Phys. Rev. Lett.* **2011**, *106*, 030802.

(37) Taylor, J. M.; Cappellaro, P.; Childress, L.; Jiang, L.; Budker, D.; Hemmer, P. R.; Yacoby, A.; Walsworth, R.; Lukin, M. D. *Nat. Phys.* **2008**, *4*, 810–816.
(38) Balasubramanian, G.; Chan, I. Y.; Kolesov, R.; Al-Hmoud, M.; Tisler, J.; Shin, C.; Kim, C.; Wojcik, A.; Hemmer, P. R.; Krueger, A.; Hanke, T.; Leitenstorfer, A.; Bratschitsch, R.; Jelezko, F.; Wrachtrup, J. *Nature* **2008**, *455*, 648–652.
(39) McGuinness, L. P.; Yan, Y.; Stacey, A.; Simpson, D. A.; Hall, L. T.; Maclaurin, D.; Prawer, S.; Mulvaney, P.; Wrachtrup, J.; Caruso, F.; Scholten, R. E.; Hollenberg, L. C. L. *Nat. Nanotechnol.* **2011**, *6*, 358–363.
(40) Davies, G.; Hamer, M. F. *Proc. R. Soc. London Ser. A* **1976**, *348*, 285–298.
(41) Gruber, A.; Dräbenstedt, A.; Tietz, C.; Fleury, L.; Wrachtrup, J.; von Borczyskowski, C. *Science* **1997**, *276*, 2012–2014.
(42) Dolde, F.; Fedder, H.; Doherty, M. W.; Nobauer, T.; Rempp, F.; Balasubramanian, G.; Wolf, T.; Reinhard, F.; Hollenberg, L. C. L.; Jelezko, F.; Wrachtrup, J. *Nat. Phys.* **2011**, *7*, 459–463.
(43) Shin, C.; Kim, C.; Kolesov, R.; Balasubramanian, G.; Jelezko, F.; Wrachtrup, J.; Hemmer, P. R. *J. Lumin.* **2010**, *130*, 1635–1645.
(44) Gurudev Dutt, M. V.; Childress, L.; Jiang, L.; Togan, E.; Maze, J.; Jelezko, F.; Zibrov, A. S.; Hemmer, P. R.; Lukin, M. D. *Science* **2007**, *316*, 1312–1316.
(45) Childress, L.; Dutt, M. V. G.; Taylor, J. M.; Zibrov, A. S.; Jelezko, F.; Wrachtrup, J.; Hemmer, P. R.; Lukin, M. D. *Science* **2006**, *314*, 281–285.
(46) Griffin, R. G.; Prisner, T. F. *Phys. Chem. Chem. Phys.* **2010**, *12*, 5737–5740. Also, see the themed issue on Dynamic Nuclear Polarization, *Phys. Chem. Chem. Phys.* **2010**, *12* (22) and the special issue of *Appl. Magn. Res.* **2008**, *34* (3 and 4).
(47) Maly, T.; Debelouchina, G. T.; Bajaj, V. S.; Hu, K. N.; Joo, C. G.; Mak-Jurkauskas, M. L.; Sirigiri, J. R.; van der Wel, P. C. A.; Herzfeld, J.; Temkin, R. J.; Griffin, R. G. *J. Chem. Phys.* **2008**, *128*, 052211.
(48) Ardenkjaer-Larsen, J. H.; Fridlund, B.; Gram, A.; Hansson, G.; Hansson, L.; Lerche, M. H.; Servin, R.; Thaning, M.; Golman, K. *Proc. Natl. Acad. Sci. U.S.A.* **2003**, *100*, 10158–10163.
(49) Joo, C. G.; Hu, K. N.; Bryant, J. A.; Griffin, R. G. *J. Am. Chem. Soc.* **2006**, *128*, 9428–9432.
(50) Joo, C. G.; Casey, A.; Turner, C. J.; Griffin, R. G. *J. Am. Chem. Soc.* **2009**, *131*, 12–13.
(51) Maly, T.; Andreas, L. B.; Smith, A. A.; Griffin, R. G. *Phys. Chem. Chem. Phys.* **2010**, *12*, 5872–5878.
(52) Reynhardt, E. C.; High, G. L. *J. Chem. Phys.* **1998**, *109*, 4090–4099.
(53) Reynhardt, E. C.; High, G. L. *J. Chem. Phys.* **1998**, *109*, 4100–4107.
(54) Reynhardt, E. C.; High, G. L. *J. Chem. Phys.* **2000**, *113*, 744–750.
(55) Duijvestijn, M. J.; van der Lugt, C.; Smidt, J.; Wind, R. A.; Zilm, K. W.; Staplin, D. C. *Chem. Phys. Lett.* **1983**, *102*, 25–28.
(56) Takeda, K.; Takegoshi, K.; Terao, T. *J. Phys. Soc. Jpn.* **2004**, *73*, 2313–2318.
(57) Takeda, K.; Takegoshi, K.; Terao, T. *J. Phys. Soc. Jpn.* **2004**, *73*, 2319–2322.
(58) Goodson, B. M. *Annu. Rep. NMR Spectrosc.* **2005**, *55*, 299–323.
(59) Iinuma, M.; Takahashi, Y.; Shaké, I.; Oda, M.; Shimizu, H. M.; Masaike, A.; Yabuzaki, T. *J. Phys. Soc. Jpn.* **2005**, *9*, 2622–2630.
(60) Iinuma, M.; Takahashi, Y.; Shaké, I.; Oda, M.; Masaike, A.; Yabuzaki, T.; Shimizu, H. M. *J. Magn. Reson.* **2005**, *175*, 235–241.
(61) van Kesteren, H. W.; Wenckebach, W. Th.; Schmidt, J.; Poulis, N. J. *Chem. Phys. Lett.* **1982**, *89*, 67–70.
(62) van Kesteren, H. W.; Wenckebach, W. Th.; Schmidt, J. *Phys. Rev. Lett.* **1985**, *55*, 1642–1644.
(63) Lawler, R. G. *J. Am. Chem. Soc.* **1967**, *89*, 5519–5521.
(64) Lawler, R. G. *Acc. Chem. Res.* **1972**, *5*, 25–33.
(65) Ward, H. R. *Acc. Chem. Res.* **1972**, *5*, 18–24.
(66) Navon, G.; Song, Y.-Q.; Rõõm, T.; Appelt, S.; Taylor, R. E.; Pines, A. *Science* **1996**, *271*, 1848–1851.
(67) Goodson, B. M.; Song, Y.-Q.; Taylor, R. E.; Schepkin, V. D.; Brennan, K. M.; Chingas, G. C.; Budinger, T. F.; Navon, G.; Pines, A. *Proc. Natl. Acad. Sci. U.S.A.* **1997**, *94*, 14725–14729.
(68) Pavlovskaya, G. E.; Cleveland, Z. I.; Stupic, K. F.; Basaraba, R. J.; Meersmann, T. *Proc. Natl. Acad. Sci. U.S.A.* **2005**, *102*, 18275–18279.
(69) Reimer, J. A. *Solid State Nucl. Magn. Reson.* **2010**, *37*, 3–12.
(70) Li, B.; Coles, P.; Reimer, J. A. *Solid State Commun.* **2010**, *150*, 450–453.
(71) Tycko, R.; Barrett, S. E.; Dabbagh, G.; Pfeiffer, L. N.; West, K. W. *Science* **1995**, *268*, 1460–1463.
(72) Barrett, S. E.; Tycko, R.; Pfeiffer, L. N.; West, K. W. *Phys. Rev. Lett.* **1994**, *72*, 1368–1371.
(73) Zhou, J.; Li, L.; Hu, H.; Yang, B.; Dan, Z.; Qiu, J.; Guo, J.; Chen, F.; Ye, C. *Solid State Nucl. Magn. Reson.* **1994**, *3*, 339–351.
(74) Acosta, V. M.; Bauch, E.; Ledbetter, M. P.; Waxman, A.; Bouchard, L.-S.; Budker, D. *Phys. Rev. Lett.* **2010**, *104*, 070801.
(75) Panich, A. M.; Shames, A. I.; Medvedev, O.; Osipov, V. Yu.; Aleksenskiy, A. E.; Vul', A. Ya. *Appl. Magn. Reson.* **2009**, *36*, 317–329.
(76) Shames, A. I.; Panich, A. M.; Osipov, V. Yu.; Aleksenskiy, A. E.; Vul', A. Ya.; Enoki, T.; Takai, K. *J. Appl. Phys.* **2010**, *107*, 014318.
(77) Panich, A. M.; Vieth, H.-M.; Shames, A. I.; Froumin, N.; Osawa, E.; Yao, A. *J. Phys. Chem. C* **2010**, *114*, 774–782.
(78) Dubois, M.; Guérin, K.; Petit, E.; Batisse, N.; Hamwi, A.; Komatsu, N.; Giraudet, J.; Pirotte, P.; Masin, F. *J. Phys. Chem. C* **2009**, *113*, 10371–10378.
(79) Belobrov, P. I.; Gordeev, S. K.; Petrakovskaya, É. A.; Falaleev, O. V. *Dokl. Phys.* **2001**, *46*, 459–462.
(80) Fang, X. W.; Mao, J. D.; Levin, E. M.; Schmidt-Rohr, K. *J. Am. Chem. Soc.* **2009**, *131*, 1426–1435.
(81) Levin, E. M.; Fang, X. W.; Bud'ko, S. L.; Straszheim, W. E.; McCallum, R. W.; Schmidt-Rohr, K. *Phys. Rev. B* **2008**, *77*, 054418.
(82) Shames, A. I.; Osipov, V. Yu.; Aleksenskiy, A. E.; Ōsawa, E.; Vul', A. Ya. *Diamond Relat. Mater.* **2011**, *20*, 318–321.
(83) Panich, A. M.; Shames, A. I.; Vieth, H.-M.; Osawa, E.; Vul, A. Ya. *Eur. Phys. J. B* **2006**, *52*, 397–402.
(84) Rovere, M.; Porro, S.; Musso, S.; Shames, A.; Williams, O.; Bruno, P.; Tagliaferro, A.; Gruen, D. M. *Diamond Relat. Mater.* **2006**, *15*, 1913–1916.